Scripta Materialia 130 (2017) 182–186

Contents lists available at ScienceDirect

Scripta Materialia

journal homepage: www.elsevier.com/locate/scriptamat

Regular article

Size and strain rate effects in metallic samples of confined volumes: Dislocation length distribution

George Z. Voyiadjis *, Mohammadreza Yaghoobi

Computational Solid Mechanics Laboratory, Department of Civil and Environmental Engineering, Louisiana State University, Baton Rouge, LA 70803, United States

ARTICLE INFO

Article history:
Received 28 October 2016
Accepted 2 December 2016
Available online xxxx

Keywords:
Size effects
Strain rate
Molecular dynamics
Dislocation
Compression test

ABSTRACT

In metallic samples of confined volumes, the size effects are governed by the characteristics of the dislocation network. However, there are only few studies that quantitatively tried to relate the dislocation network properties to the sample size effects. The present work studies the dislocation length distribution in pillars with different sizes during compression test with different strain rates using large scale atomistic simulation. The size and strain rate effects are then investigated using the observed dislocation length distribution.

The most common experiment to investigate the size effects in samples of confined volumes is the micropillar compression test, which was introduced by Uchic et al. [1,2]. During the micropillar compression test, the sample is subjected to the uniform loading and in the absence of any strain gradients, the size effects are solely originated from the size of the tested pillars. Size effects in metallic samples of confined volume have been attributed to the different mechanisms of dislocation starvation, source exhaustion, and the effect of dislocation source length [3,4]. In the case of the latter mechanism, the strength of the sample is controlled by the longest dislocation source, which is the first dislocation activated by the applied stress. Parthasarathy et al. [5] presented an equation to describe the probability for the maximum distance from the pin to the free surface that leads to the longest dislocation arm. They also proposed an equation to incorporate the dislocation source length into the calculation of critical resolved shear strength (CRSS) [5]. Rao et al. [6] incorporated 3-D discrete dislocation dynamics (DDD) and investigated the athermal mechanisms of size effects during the micropillar compression test. They reported the values of largest source length for 26 different samples with the same size and initial dislocation density [6]. El-Awady et al. [7] investigated the size effects using 3-D DDD and observed that the mean dislocation length governs the size effects. They incorporated a random dislocation length distribution that follows the two-parameter Weibull distribution [7]. El-Awady et al. [7] observed that to reproduce the experimental results obtained by Dimiduk et al. [8] and Frick et al. [9], the mean length of dislocation should be chosen equal to the $D/25$ which D is the pillar diameter. They also observed that the dislocation lengths close to the pillar diameter are rare [7]. Cui et al. [10] studied the dislocation source as the governing mechanism of size effects using 3-D DDD. They measured the stable source lengths for samples with various sizes and observed that the average stable source lengths is a function of sample diameter (Cui et al. [10]). El-Awady [11] conducted 3-D DDD simulations of pillars with various sizes and initial dislocation densities and captured the variation of mean dislocation length using the sample size and initial dislocation density. The dislocation length distribution has been extensively studied for bulk materials [7,12,13,14]. However, it has not been investigated for samples of confined volumes. In the current study, the size and strain rate effects are presented during the micropillar compression test. The results show that increasing the strain rate decreases the size effects. Next, it is shown that the dislocation density is not the appropriate parameter for studying size effects in samples of confined volumes. Finally, the dislocation length distribution is investigated for pillars of different sizes subjected to the compression loading of various strain rates. The size and strain rate effects are captured using the observed dislocation network properties. It is shown that in the cases of the studied samples, one should incorporate the largest dislocation length and not the mean dislocation length to capture the size and strain rate effects.

The first mathematical prediction of effective dislocation source length was proposed by Parthasarathy et al. [5]. They introduced the

* Corresponding author.
E-mail address: voyiadjis@eng.lsu.edu (G.Z. Voyiadjis).

http://dx.doi.org/10.1016/j.scriptamat.2016.12.001
1359-6462/

probability of a cylindrical sample with n pins to have the maximum distance from the free surface equal to λ_{max} as follows [5]:

$$p(\lambda_{max})d\lambda_{max} = \left[1-\frac{\pi(R-\lambda_{max})(b-\lambda_{max})}{\pi Rb}\right]^{n-1}\left(\frac{\pi[(R-\lambda_{max})+(b-\lambda_{max})]}{\pi Rb}\right)nd\lambda_{max} \quad (1)$$

where R is the specimen radius, $b = R/\cos\beta$ is the major axis of the glide plane, and β is the angle between the primery slip plane and the loading axis. Using the probability function defined in Eq. (1), the mean effective source length $\overline{\lambda}_{max}$ can be obtained as below [5]:

$$\overline{\lambda}_{max} = \int_0^R \lambda_{max}p(\lambda_{max})d\lambda_{max} = \int_0^R \left[1-\frac{\pi(R-\lambda_{max})(b-\lambda_{max})}{\pi Rb}\right]^{n-1}\left(\frac{\pi[(R-\lambda_{max})+(b-\lambda_{max})]}{\pi Rb}\right)n\lambda_{max}d\lambda_{max} \quad (2)$$

In the next step, the CRSS was related to $\overline{\lambda}_{max}$ as follows:

$$\text{CRSS} = \frac{\alpha Gb}{\overline{\lambda}_{max}} + \tau_0 + 0.5Gb\sqrt{\rho} \quad (3)$$

where α is a constant, G is the shear modulus, b is the Burgers vector, τ_0 is the friction stress, and ρ is the dislocation density. The number of pins, n, is also predicted as follows [5]:

$$n = \text{Integer}\left[\frac{L_{mobile}}{L_{ave}}\right] \quad (4)$$

where L_{ave} is the average length of dislocation segments, $L_{mobile} = \rho\pi R^2 h/s$ is the total length of mobile dislocations, h is the height of the pillar, and s is the number of slip systems. Basically, Parthasarathy et al. [5] and later Rao et al. [6] related the size effects to the average largest source length $\overline{\lambda}_{max}$. El-Awady and his coworkers [7,11,15] related the size effects to the mean dislocation length L_{ave}. El-Awady [11] proposed an equation to obtain L_{ave} using the pillar diameter and initial dislocation density ρ_0 as follows:

$$L_{ave} = \frac{bD\sqrt{\rho_0}}{\overline{\beta}} \quad for\ \rho_0 < \rho_0^{cr} \quad (5a)$$

$$L_{ave} = \frac{1}{\overline{\alpha}\sqrt{\rho_0}} \quad for\ \rho_0 \geq \rho_0^{cr} \quad (5b)$$

where ρ_0^{cr} is the critical initial dislocation density at which L_{ave} becomes independent of sample size, and $\overline{\alpha}$ and $\overline{\beta}$ are dimensionless constants.

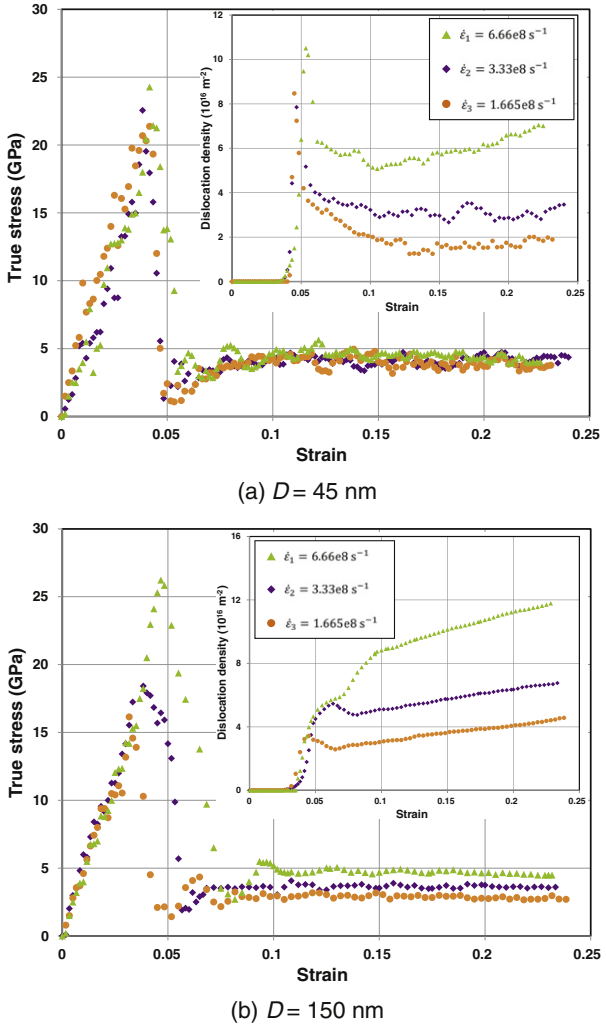

Fig. 1. The compressive responses of pillars at different strain rates of $\dot{\varepsilon}_1 = 6.66e8\ s^{-1}$, $\dot{\varepsilon}_2 = 3.33e8\ s^{-1}$, and $\dot{\varepsilon}_3 = 1.665e8\ s^{-1}$ with the diameters of: (a) $D = 45$ nm (b) $D = 150$ nm.

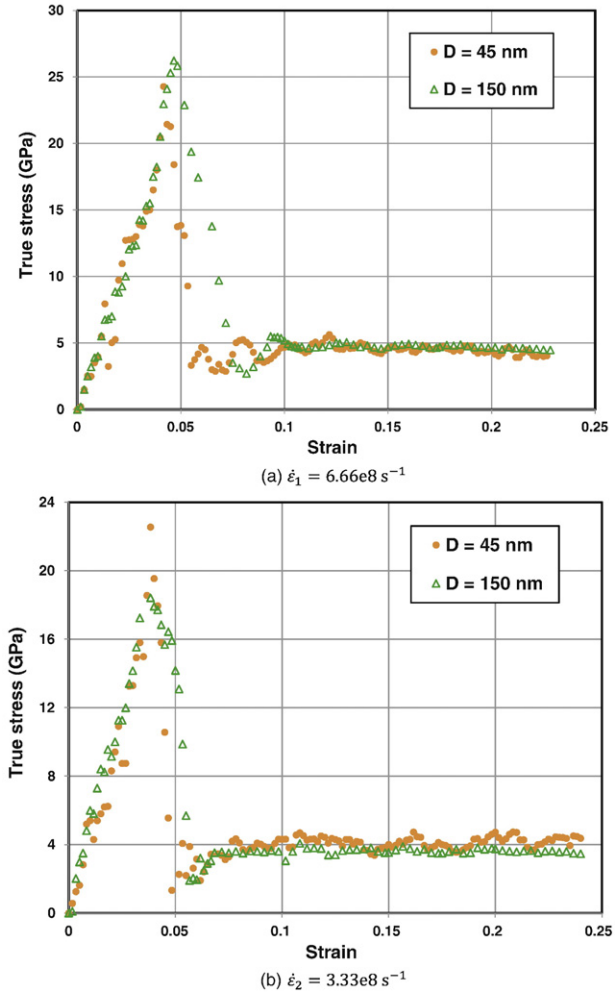

Fig. 2. Variation of true stress versus the strain in the cases of the pillars with the diameters of 45 nm and 150 nm at different strain rates of: (a) $\dot{\varepsilon}_1 = 6.66e8\ s^{-1}$ (b) $\dot{\varepsilon}_2 = 3.33e8\ s^{-1}$ (c) $\dot{\varepsilon}_3 = 1.665e8\ s^{-1}$.

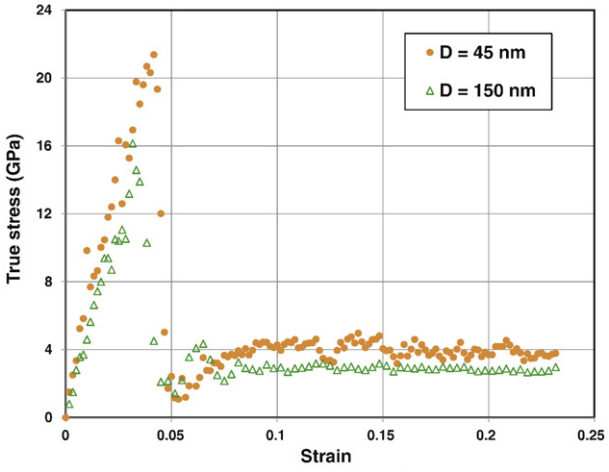

Fig. 2 (*continued*).

In the current study, the molecular dynamics (MD) simulation is performed using the parallel code LAMMPS [16] to study the size and strain rate effects. The embedded-atom method (EAM) potential developed by Mishin et al. [17] is used to model the Ni-Ni atomic interaction [18]. Two pillar with circular cross section, heights of 90 nm and 300 nm, and aspect ratio of *Length:Diameter* = 2:1 are modeled, which consist of 13 million and 487 million atoms, respectively. The axis of pillars is along the [1 1 1] direction. The boundary conditions are selected similar to the one described by Yaghoobi and Voyiadjis [19] in which the top and bottom surfaces are set free. A prescribed potential wall is incorporated to simulate the substrate. A large flat indenter is used to impose the compressive displacement with three strain rates of $\dot{\varepsilon}_1 = 6.66e8\ s^{-1}$, $\dot{\varepsilon}_2 = 3.33e8\ s^{-1}$, and $\dot{\varepsilon}_3 = 1.665e8\ s^{-1}$, which are in the common range of applied strain rates of the previous works [19,20,21]. The following repulsive potential is incorporated to model the interaction between the indenter and Ni atoms [22]:

$$E^{\text{ind}}(r) = \bar{\varepsilon}_{\text{ind}}(r - r_c)^2 \quad r < r_c \tag{6}$$

where $\bar{\varepsilon}_{\text{ind}} = 1\ \text{eV/Å}^2$, r, and $r_c = 0.3$ nm are the specified force constant, distance from particle to the indenter surface, and cutoff distance, respectively. The Si substrate is modeled using the Lennard–Jones (LJ) potential as follows [22]:

$$E^{\text{LJ}}(r_{ij}) = 4\bar{\varepsilon}\left[\left(\frac{\bar{\sigma}}{r_{ij}}\right)^{12} - \left(\frac{\bar{\sigma}}{r_{ij}}\right)^{6}\right] \tag{7}$$

where $\bar{\sigma}$ is the collision diameter at which $E^{\text{LJ}} = 0$, and $\bar{\varepsilon}$ is the depth of the potential well. The LJ parameters are $\bar{\varepsilon}_{\text{Ni-Si}} = 1.5231e{-}20$ J and $\bar{\sigma}_{\text{Ni-Si}} = 3.0534$ Å with the cutoff distance equal to $2.5\bar{\sigma}$ [22]. The velocity Verlet algorithm with the time step of 5 fs is used to numerically integrate the equations of Motion The simulation is conducted using the NVT ensemble [16]. The triangulation method [22–25] is incorporated to capture the precise cross section area during the simulation. The crystal Analysis tool [26–29] is used to extract the dislocation structure from the atomic trajectories. The dislocation network is visualized and analyzed using the software Paraview [30] and OVITO [31].

Since the samples are initially defect free at the start of MD simulation, which is not true in the real experiments, the stress after the initial nucleation is incorporated to study the size effects (see e.g. [19]). Fig. 1 (a) presents the variations of true stress (σ) and dislocation density (ρ) versus the strain (ε) in the case of the smaller pillar at three different strain rates of $\dot{\varepsilon}_1 = 6.66e8\ s^{-1}$, $\dot{\varepsilon}_2 = 3.33e8\ s^{-1}$, and $\dot{\varepsilon}_3 = 1.665e8\ s^{-1}$. Fig. 1 (a) shows that in the case of the smaller pillar, the sample strength is nearly independent of the strain rate. However, the dislocation density increases as the strain rate increases. The results indicate that the dislocation density is not an appropriate measure to study the size effects in the case of metallic samples of confined volumes. Fig. 1 (b) presents the $\sigma-\varepsilon$ and $\rho-\varepsilon$ in the case of the larger pillar at three different strain rates of $\dot{\varepsilon}_1 = 6.66e8\ s^{-1}$, $\dot{\varepsilon}_2 = 3.33e8\ s^{-1}$, and $\dot{\varepsilon}_3 = 1.665e8\ s^{-1}$. The dislocation density shows a similar trend compared to that of the smaller sample as the strain rate varies. However, the results show that the strength of the sample decreases by decreasing the strain rate. Fig. 2 compares the responses of pillars with different sizes during the compression test for different strain rates. The results show that as the strain rate increases, less size effects are observed in the simulated samples. In other words, increasing the strain rate decreases the size effects.

In order to capture the observed results, the dislocation length distribution is studied for different sample sizes subjected to various strain rates. The distribution of each sample is obtained by averaging the distributions at five strain values of 0.1, 0.125, 0.15, 0.175, and 0.2. Fig. 3 presents the variation of probability density function (PDF) versus the dislocation link length in both pillar sizes at different strain rates. The vertical axis of Fig. 3, i.e. PDF, is presented in logarithmic form. In the case of dislocation length distribution function of bulk materials, the maximum PDF occurs for some dislocation length in the middle of the

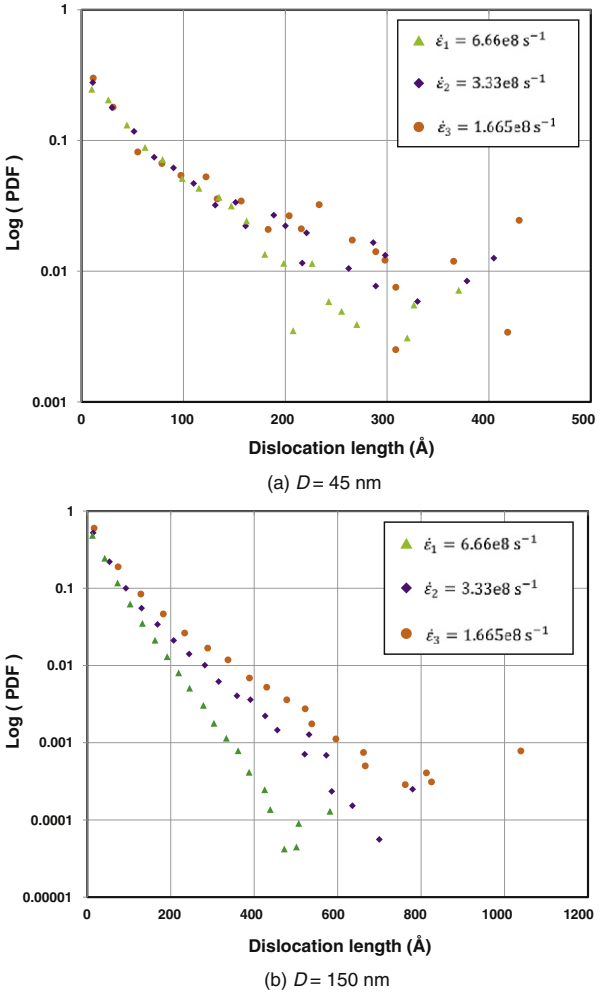

Fig. 3. Probability distribution function of dislocation lengths at different strain rates of $\dot{\varepsilon}_1 = 6.66e8\ s^{-1}$, $\dot{\varepsilon}_2 = 3.33e8\ s^{-1}$, and $\dot{\varepsilon}_3 = 1.665e8\ s^{-1}$ in the cases of pillars with the diameters of: (a) $D = 45$ nm (b) $D = 150$ nm.

distribution, and the dislocation length distribution can be approximated by a Weibull distribution function, see e.g. El-Awady et al. [7]. In the case of samples of confined volumes, however, the results show that most of the dislocation lengths are populated in the first length bean, which has the smallest length. In other words, the maximum PDF occurred at the smallest dislocation length bean. It is due to the activity of cross-slip as the major deformation mechanism in the samples with confined volumes [19]. To verify the proposed description, the dislocation visualization of both pillar sizes at $\varepsilon = 0.2$ for strain rate of $\dot{\varepsilon}_2$ is presented as an example in Fig. 4. The visualization results show that the main mechanism of deformation is cross-slip which produces many small dislocations. A similar trend can be observed in the results obtained by Hussein et al. [32] in which many small dislocations are produced by incorporating the cross-slip in the DDD formulation.

In the case of the smaller pillar, the values of average dislocation length L_{ave} are 25.29 Å, 27.03 Å, and 27.2 Å at strain rates of $\dot{\varepsilon}_1$, $\dot{\varepsilon}_2$, and $\dot{\varepsilon}_3$, respectively. In the case of the larger sample, the average dislocation length values are 21.09 Å, 23.2 Å, and 24.75 Å at strain rates of $\dot{\varepsilon}_1$, $\dot{\varepsilon}_2$, and $\dot{\varepsilon}_3$, respectively. As described by El-Awady [11], L_{ave} can be a function of dislocation density and sample size depending on the dislocation density of the sample. Considering the order of dislocation density which is 10^{16} m^{-2}, the L_{ave} should follow Eq. (5b) in which the L_{ave} is independent of the sample size and has an inverse relation with the dislocation density. The results show that L_{ave} independent of the sample size, i.e. L_{ave} of the larger pillar are close to that of the smaller one and even the smaller pillar has slightly larger L_{ave}. Also, as the strain rate increases, L_{ave} decreases which is due to the fact that increasing the strain rate increases the dislocation density. Eq. (5), which was proposed by El-Awady [11], can be micromechanically justified based on the dislocation network characteristics. In the region of small dislocation densities, i.e. Eq. (5a), increasing the sample size and dislocation density increases the chance of larger dislocation formation. In the region of high dislocation densities, however, increasing the dislocation density increases the chance of dislocations colliding with each other and dislocation refinement which decrease the dislocation length and consequently L_{ave}.

The values of the $\frac{(L_{ave})_{\dot{\varepsilon}_3}}{(L_{ave})_{\dot{\varepsilon}_1}}$ for smaller and larger pillars are 1.08 and 1.17 which are very close to each other. However, the strength of the smaller sample does not change as the strain rate varies while the larger sample inhibits significant strain rate effects. The results show that the strain rate effects cannot be captured using L_{ave}. Another way to reach the same conclusion is since L_{ave} is a function of dislocation density, and dislocation density variation is not capable of capturing size effects as shown in Fig. 1. Accordingly, L_{ave} is also not an appropriate dislocation network property to study the size effects.

Another dislocation network property which can be incorporated to study the size effects is the largest dislocation length L_{max}. Here, the L_{max} is averaged at five strain values of 0.1, 0.125, 0.15, 0.175, and 0.2 for each pillar size and strain rate. The values of L_{max} for the smaller sample and different rates of $\dot{\varepsilon}_1$, $\dot{\varepsilon}_2$, and $\dot{\varepsilon}_3$ are 377.9 Å, 415 Å, and 432.9 Å, respectively. In the case of the larger sample, L_{max} values are 605.8 Å, 783.4 Å, and 1095.6 Å for strain rates of $\dot{\varepsilon}_1$, $\dot{\varepsilon}_2$, and $\dot{\varepsilon}_3$, respectively. The values of the $\frac{(L_{max})_{\dot{\varepsilon}_3}}{(L_{max})_{\dot{\varepsilon}_1}}$ for smaller and larger pillars are 1.14 and 1.81 which shows a great difference compared to the values of $\frac{(L_{ave})_{\dot{\varepsilon}_3}}{(L_{ave})_{\dot{\varepsilon}_1}}$. As an example, in the case of Fig. 4, the true stresses for smaller and larger pillars at $\varepsilon = 0.2$ and strain rate of $\dot{\varepsilon}_2$ are $\sigma_{D=45\ nm} = 4.72$ GPa and

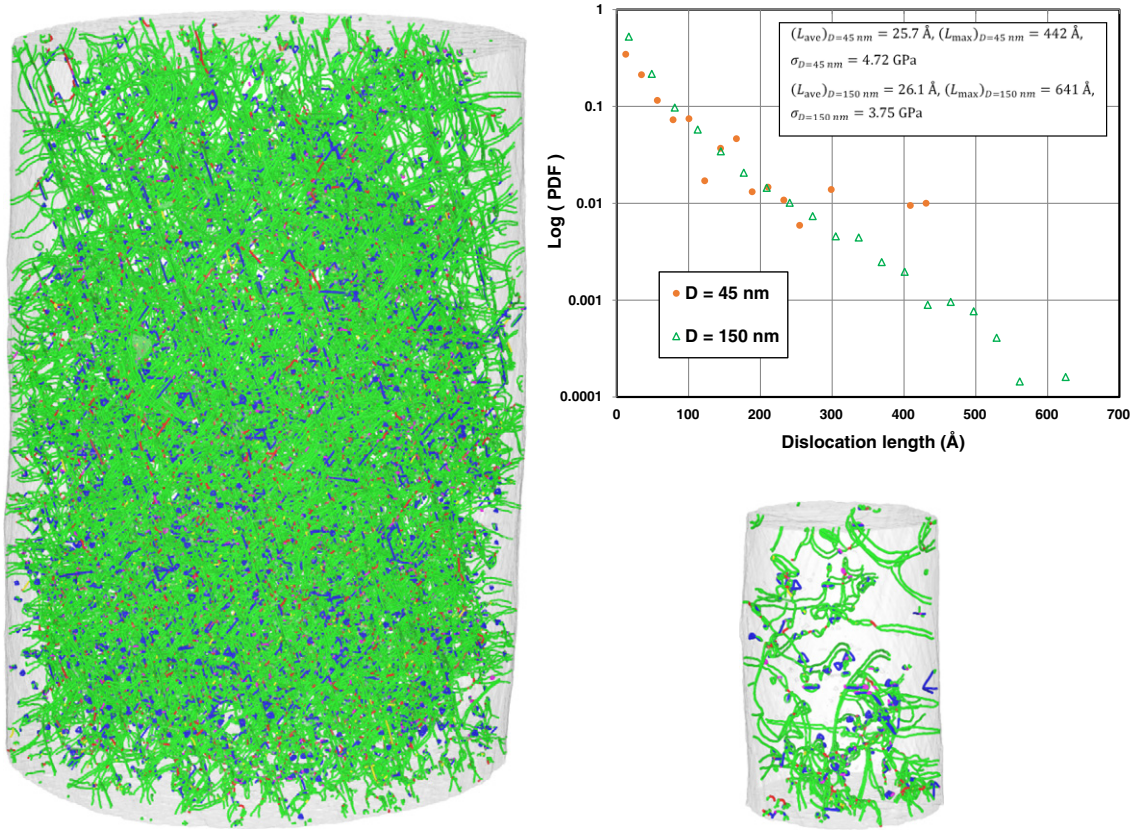

Fig. 4. The dislocation network at $\varepsilon = 0.2$ for the strain rate of $\dot{\varepsilon}_2 = 3.33e8\ s^{-1}$ and pillar diameters of: (a) $D = 150$ nm (b) $D = 45$ nm.

$\sigma_{D=150\ nm} = 3.75$ GPa, respectively, where $\sigma_1/\sigma_2 = 1.26$. The average dislocation length for the smaller and larger pillars are $(L_{ave})_{D=45\ nm} = 25.7$ Å and $(L_{ave})_{D=150\ nm} = 26.1$ Å, respectively, which are nearly similar. The maximum dislocation length, on the other hand, for the smaller and larger samples are $(L_{max})_{D=45\ nm} = 442$ Å and $(L_{max})_{D=150\ nm} = 641$ Å, respectively, which shows that the sample with smaller L_{max} has the larger strength. The results show that the maximum dislocation length L_{max} is the appropriate dislocation network property to study the size effects and not the L_{ave}. It is due to the fact that there are tremendous small dislocations induced by the cross-slip in the samples of confined volumes, which was also observed by Hussein et al. [32]. Accordingly, the average dislocation length is highly influenced by the small dislocations, and the effect of maximum source length on L_{ave} diminishes. The maximum dislocation length L_{max}, on the other hand, is fully capable of capturing size and strain rate effects. For example, the results observed in Fig. 2 can be fully explained by L_{max}. The L_{max} in the larger pillar divided by that of the smaller pillar is 1.6, 1.89, and 2.53 at different strain rates of $\dot{\varepsilon}_1, \dot{\varepsilon}_2$, and $\dot{\varepsilon}_3$ which shows that increasing the strain rate decreases the size effects by decreasing the difference between the L_{max} for samples of different sizes. The obtained results are important for many applications such as electronic packaging, where material properties are obtained from large samples in centimeters, however, the actual structures are in microns and nanometers [33,34].

This research was conducted with high performance computing resources provided by Louisiana State University (http://www.hpc.lsu.edu) and Louisiana Optical Network Initiative (http://www.loni.org). The current work is partially funded by the NSF EPSCoR CIMM project under award #OIA-1541079.

References

[1] M.D. Uchic, D.M. Dimiduk, J.N. Florando, W.D. Nix, Mater. Res. Soc. Symp. Proc. 753 (2003) 27–32.
[2] M.D. Uchic, D.M. Dimiduk, J.N. Florando, W.D. Nix, Science 305 (2004) 986–989.
[3] M.D. Uchic, P.A. Shade, D.M. Dimiduk, Annu. Rev. Mater. Res. 39 (2009) 361–386.
[4] O. Kraft, P. Gruber, R. Mönig, D. Weygand, Annu. Rev. Mater. Res. 40 (2010) 293–317.
[5] T.A. Parthasarathy, S.I. Rao, D.M. Dimiduk, M.D. Uchic, D.R. Trinkle, Scr. Mater. 56 (2007) 313–316.
[6] S.I. Rao, D.M. Dimiduk, T.A. Parthasarathy, M.D. Uchic, M. Tang, C. Woodward, Acta Mater. 56 (2008) 3245–3259.
[7] J.A. El-Awady, M. Wen, N.M. Ghoniem, J. Mech. Phys. Solids 57 (2009) 32–50.
[8] D. Dimiduk, M. Koslowski, R. LeSar, Scr. Mater. 53 (2005) 4065–4077.
[9] C. Frick, B. Clark, S. Orso, A. Schneider, E. Arzt, Mater. Sci. Eng. A 489 (2008) 319–329.
[10] Y.N. Cui, P. Lin, Z.L. Liu, Z. Zhuang, Int. J. Plast. 55 (2014) 279–292.
[11] J.A. El-Awady, Nat. Commun. 6 (2014) 5926.
[12] P. Lin, S.S. Lee, A.J. Ardell, Acta Metall. 37 (1989) 739–748.
[13] H. Mughrabi, J. Microsc, Spectrosc. Electron 1 (1976) 571–584.
[14] A.J. Ardell, S.S. Lee, Acta Metall. 34 (1986) 2411–2423.
[15] J.A. El-Awady, S.B. Biner, N.M. Ghoniem, J. Mech. Phys. Solids 56 (2008) 2019–2035.
[16] S. Plimpton, J. Comput. Phys. 117 (1995) 1–19.
[17] Y. Mishin, D. Farkas, M.J. Mehl, D.A. Papaconstantopoulos, Phys. Rev. B 59 (1999) 3393–3407.
[18] C.A. Becker, F. Tavazza, Z.T. Trautt, R.A. Buarque de Macedo, Curr. Opin. Solid State Mater. Sci. 17 (2013) 277–283http://www.ctcms.nist.gov/potentials.
[19] M. Yaghoobi, G.Z. Voyiadjis, Acta Mater. 121 (2016) 190–201.
[20] G.J. Tucker, Z.H. Aitken, J.R. Greer, C.R. Weinberger, Model. Simul. Mater. Sci. Eng. 21 (2013) 015004.
[21] S. Xu, Y.F. Guo, A.H.W. Ngan, Int. J. Plast. 43 (2013) 116–127.
[22] M. Yaghoobi, G.Z. Voyiadjis, Comput. Mater. Sci. 95 (2014) 626–636.
[23] G.Z. Voyiadjis, M. Yaghoobi, Mater. Sci. Eng. A 634 (2015) 20–31.
[24] M. Yaghoobi, G.Z. Voyiadjis, Comput. Mater. Sci. 111 (2016) 64–73.
[25] G.Z. Voyiadjis, M. Yaghoobi, Comput. Mater. Sci. 117 (2016) 315–329.
[26] A. Stukowski, Model. Simul. Mater. Sci. Eng. 20 (2012) 045021.
[27] A. Stukowski, K. Albe, Model. Simul. Mater. Sci. Eng. 18 (2010) 085001.
[28] A. Stukowski, V.V. Bulatov, A. Arsenlis, Model. Simul. Mater. Sci. Eng. 20 (2012) 085007.
[29] A. Stukowski, JOM 66 (2014) 399–407.
[30] A. Henderson, Paraview guide, A Parallel Visualization Application, Kitware Inc, 2007http://www.paraview.org.
[31] A. Stukowski, Model. Simul. Mater. Sci. Eng. 18 (2010) 015012http://www.ovito.org/.
[32] A. Hussein, S. Rao, M. Uchic, D. Dimiduk, J. El-Awady, Acta Mater. 85 (2015) 180–190.
[33] C. Basaran, J. Jiang, Mech. Mater. 34 (2002) 349–362.
[34] J. Gomez, C. Basaran, Int. J. Solids Struct. 43 (2006) 1505–1527.